Ahmadu *et al.*
Journal of Engineering and Applied Science (2022) 69:63
https://doi.org/10.1186/s44147-022-00116-1

Journal of Engineering and Applied Science

RESEARCH Open Access

Experimental evaluation of a modified direct evaporative cooling system combining luffa fiber—charcoal cooling pad and activated carbon dehumidifying pad

T. O. Ahmadu*, Y. S. Sanusi and F. Usman

*Correspondence: talibahmadu@gmail.com

Department of Mechanical Engineering, Faculty of Engineering, Ahmadu Bello University, Zaria, Nigeria

Abstract

Evaporative cooling technology has a potential to serve as a substitute to conventional vapor compression cooling. Direct evaporative cooling however usually introduces more moisture to the cooling space. In this study, the performance of a modified direct evaporative cooling system that combines a cooling pad and a removable dehumidifying pad has been experimentally evaluated for space cooling. The cooling pad is made of luffa fiber lagged with charcoal, while the dehumidifying pad is made of activated carbon derived from tamarind seed. Results for two experimental days, which span from 8:30 am to 5:30 pm each day are reported in this work. The peak cooling load requirement of the room was evaluated as 4.53 kW. On the first experimental day, in which the dehumidifying pad was removed from the system, results indicated a minimum room temperature of 24 °C was achieved, which resulted in a maximum temperature drop of 11 °C from ambient temperature. However, indoor relative humidity increased to a maximum of 84%, while outdoor relative humidity was 30%. The dehumidifying pad was used on the second experimental day. Results from the second experimental day showed a minimum room temperature of 26.5 °C was achieved, resulting in a maximum temperature drop of 10 °C from ambient. Maximum indoor relative humidity recorded was 49%, while the outdoor relative humidity was 34%, an indication that the dehumidifying pad was able to absorb moisture from the cooled air. Maximum cooling capacity, efficiency, and COP of 3.84 kW, 84.6% and 16.1 respectively were achieved by the system without the dehumidifying pad. Corresponding values of 3.2 kW, 71.4% and 13.4 respectively were recorded when the system was operated with the dehumidifying pad.

Keywords: Evaporative cooling, Cooling pad, Dehumidifying pad, Luffa–fiber, Activated carbon

Introduction

The increasing demand for human thermal comfort in buildings has led to increased energy consumption, with over 30% of the total world energy consumption being by air conditioning systems [1]. Over the decades, vapor compression systems are the most commonly used for air conditioning of buildings. However, major disadvantages associated with these systems include high power consumption as a result of operating the mechanical compressor and global warming tendencies due to the synthetic refrigerants used [2]. Due to these challenges, research works to develop new air conditioning technologies have been on the increase [3]. Evaporative cooling technology is a promising alternative to vapor compression cooling, due to its ability to provide thermal comfort with minimal power consumption and without the use of environmental degrading refrigerants [4]. Evaporative cooling systems employ water as refrigerant, thereby making it environmentally friendly and also do not make use of mechanical compressors, thereby reducing power consumption [5]. In evaporative cooling, water flows over a cooling pad to cool a stream of hot dry ambient air pulled through the pad. The hot dry air loses its sensible heat to the water through evaporation and results into cool humid air [6]. However, when the ambient air is humid, less water can be evaporated into the air, this leads to decreased cooling capacity.

Two major technologies are involved in evaporative cooling: direct evaporative cooling and indirect evaporative cooling [7]. Theoretically, both technologies can reduce the indoor air temperature to the outdoor wet bulb temperature. Direct evaporative cooling system is simpler in design than indirect evaporative cooling system. In direct evaporative cooling, the air to be cooled is in direct contact with water at the cooling pad; hence, it introduces extra moisture to the cooling space [7]. Introduction of extra moisture in cooling space leads to increase in humidity within the space, which could lead to major health effects on inhabitants [8]. In the case of indirect evaporative cooling, there is no direct contact of the air to be cooled with water. It employs a heat exchanger with two adjacent air streams, which together achieve cool and dry air supply to the cooling space. Hence, there is no introduction of extra moisture to the cooling space [8].

Removal of moisture from air is achieved through a dehumidifying process. The dehumidifying process is usually achieved by the use of a solid desiccant, which is a material that has ability to attract and hold water vapor [9]. One of such systems is the solid desiccant wheel in a desiccant cooling system. The wheel rotates continuously and is traversed by two streams of air flow which simultaneously achieve dehumidification and regeneration [8]. Both the indirect evaporative cooling and the desiccant cooling systems are however more complex in design than the direct evaporative cooling system. The desiccant cooling system also has more power requirements, while poor heat transfer rates and low wet bulb effectiveness are still challenges faced by the indirect evaporative cooling system [10].

Due to the high prospects of evaporative cooling technology, several research works are being conducted in this area, all aimed at improving the system performance. Ibrahim et al., [11] evaluated the performance of a direct evaporative cooling system supported with porous ceramic evaporators. Results indicated a drop in indoor dry bulb temperature between 6 and 8 °C, while indoor relative humidity increased by 30%. Maximum cooling achieved was 224 W/m^2. Awofa et al. [12] carried out a performance

evaluation of a constructed evaporative cooling system for tomatoes storage. Average temperature in the cooling compartment was 23 °C, compared to an average ambient temperature of 33 °C. Cooling efficiency of 81% was achieved and relative humidity recorded in the cooling compartment was 99% compared to an outdoor relative humidity of 59%. Abaranji et al., [6] studied the performance of a vermicompost based direct evaporative cooling system. Average temperature drop of 9.5°C and effectiveness of 80% were recorded. Increase in relative humidity of the cooling space was also recorded. Several researchers have also studied the performance of evaporative cooling systems using different cooling pad materials: Al–Sulaiman [13], used fibers of date palm, luffa, and jute. Jain and Hindoliya [14], used coconut and polash fibers. Dogramaci et al. [15] used eucalyptus fibers. Other cooling pad materials studied include pottery rods, wood chips, cotton fiber, cellulose paper, bulk charcoal, vegetable loofa [16–21]. Review of different cooling pad materials can be found in the work of Tejero–Gonzalez and Franco–Salas [22]. Solid desiccants that have been used for air conditioning applications include; silica gels, zeolites, activated alumina, molecular sieves, and activated carbon [23].

Zaher et al. [24] developed a new configuration of a desiccant evaporative cooling system using direct/ indirect cooler. Performance simulation was done using the transient systems simulation software (TRNSYS). The new configuration was found to record higher performance over the previously existing configurations. Narayanan et al. [25] used TRNSYS software to evaluate the performance of a desiccant evaporative cooling system for a residential building in Brisbane. Results showed the system could provide thermal comfort for about 50% of the time. Research works have also been conducted on direct evaporative cooling for thermal comfort in small scale residential and office buildings in different climates. Dhamneya et al., [26] carried out a theoretical performance analysis of direct evaporative system using aspen fiber cooling media of six different geometrical configurations. It was concluded that the triangular cooling media configuration attained the highest saturation efficiency of 97%. Selami et al. [27] developed a mathematical model to evaluate the performance of direct evaporative cooler that makes use of porous ceramic plates as wet media. The finite volume method was used to solve the model. Results indicate that the cooler could satisfy the cooling requirements in the arid climate with a temperature drop of 15 °C below the ambient. Khater [28] developed a mathematical model to optimize the parameters affecting performance of evaporative cooling system. The model was validated with experimental work conducted under Egyptian climatic conditions and there was good agreement between model and experimental results. He et al. [29] developed an evaporative cooling system that employs a solar energy powered reel dehumidifying system to pre-treat the outdoor fresh air. Experimental results indicate that the indoor temperature was decreased to below 28 °C, while indoor relative humidity was maintained at approximately 70%. In a study conducted by Hasani et al. [30] for effective energy, economic, and environmental cooling of small-scale residential buildings, it was suggested to implement direct evaporative cooling in all dry areas. While for temperate and humid, as well as very hot and semi humid areas, desiccant-enhanced evaporative cooling was recommended.

From the literature reviewed, not much attention has been paid to the possibility of incorporating solid desiccant into direct evaporative cooling system with the intention of eliminating the associated rise in indoor relative humidity, when used

for thermal comfort in residential buildings. In the present study, a modified direct evaporative cooling system, combining both evaporative cooling and a dehumidifying process in a simple design was developed and the performance evaluated. The system consists of a mixed media evaporative cooling pad and a passive solid desiccant dehumidifying pad, which was incorporated to remove moisture from the cooled air before passing into the cooling space. The cooling pad was made of luffa fiber combined with charcoal, while the dehumidifying pad was made of activated carbon derived from tamarind seed.

Direct evaporative cooling process

When the recirculation of water is continuous, the direct evaporative cooling process can be considered as an adiabatic process. Figure 1a shows a schematic of an evaporative cooling system. Hot ambient air is drawn by a fan (1) through a cooling pad (2). Water is circulated from a tank (3), by a pump (4) through a pipe (5) to a water sprinkler (6). The water is sprinkled over the cooling pad. Heat of vaporization is extracted from the hot ambient air which causes water to evaporate thereby cooling the air. This results in decrease in dry bulb temperature of the air, with increase in specific and relative humidity of the air. The enthalpy of the air remains constant. Figure 1b shows the process on a psychrometric chart. States 1 and 2 represent the hot ambient air and the cool moist air respectively. The air is cooled to approach the wet bulb temperature, state (3). Practically however, the air cannot be cooled below the wet bulb temperature.

Methods

The materials used and methods employed are presented in this section.

Description and operating principle of the constructed evaporative cooling system

The modified direct evaporative cooling system was designed and constructed at the department of mechanical engineering, Ahmadu Bello University, Zaria. A schematic of the system is shown in Fig. 2. It combines the normal direct evaporative cooling system, together with a passive solid desiccant dehumidification section which removes moisture from the cooled moist air. The system employs a double pad system: a mixed media cooling pad at the evaporative cooling section and a

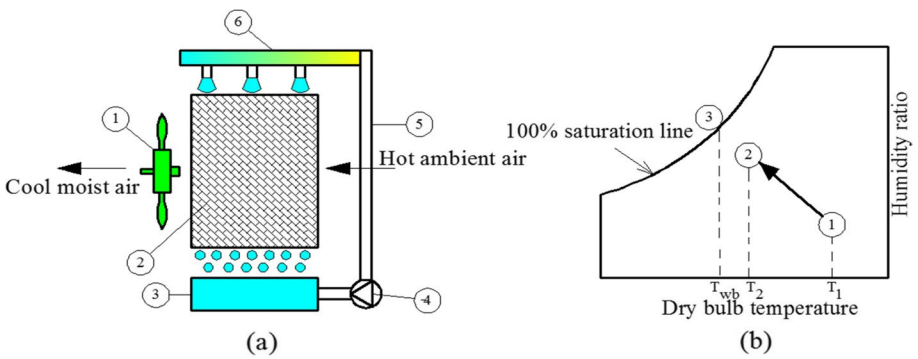

Fig. 1 **a** Schematic of direct evaporative cooling system. **b** Process on psychrometric chart

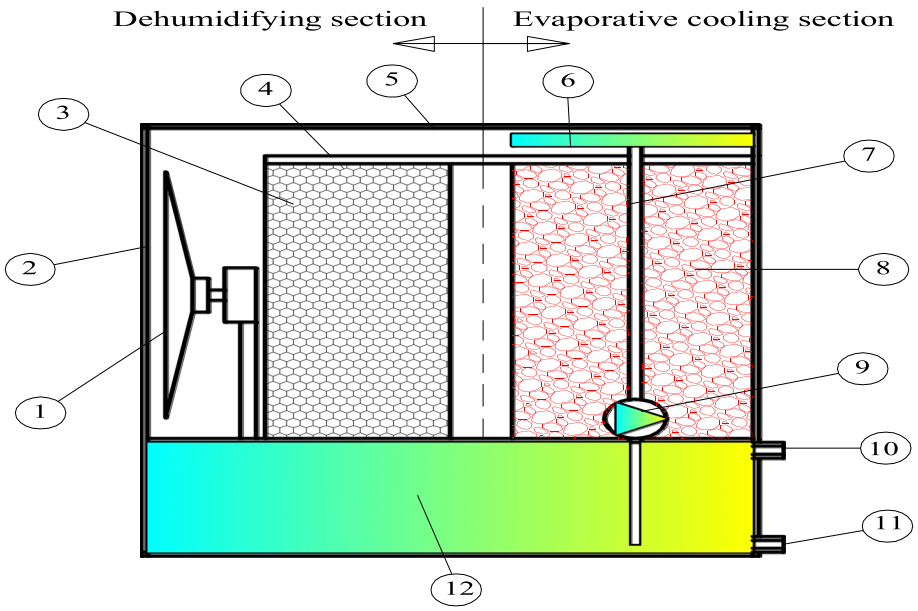

Fig. 2 Schematic of constructed modified direct evaporative cooling system

solid desiccant dehumidifying pad placed after the evaporative cooling section. Both pads are linked together in a rectangular channel (4). The system uses an electric fan (1) to suck hot ambient air first through the evaporative cooling section. Here, the air passes through the cooling pad (8), which is made of luffa sponge lagged with charcoal. Water, stored in a water storage tank (12) is circulated by a water pump (9) through PVC pipe (7) to the water spray panel (6), where it flows through series of small holes and falls by gravity through the cooling pad and returns back to the storage tank. The water in the cooling pad absorbs the heat of vaporization from the supply hot ambient air and evaporates causing the air temperature to decrease with an increase in humidity. This completes the evaporative cooling process. The resulting cool moist air is sucked by the fan through the dehumidifying pad (3). The dehumidifying pad is made of tamarind seed activated carbon granules, which is a desiccant material, capable of absorbing moisture. Moisture is absorbed at the dehumidifying pad and the resulting cool dry air flows into the cooling space. The casing (5) is made of galvanized iron sheet with angle iron as frame. Wire mesh (2) is used to protect the fan blade from direct contact. The water in the tank is refilled through the water refill pipe (10), while the water can be drained from the tank using the water drain pipe (11). Regenerating the desiccant material in the dehumidifying pad is to be done by removing the dehumidifying pad and drying in a solar dryer. Figures 3 and 4 show the constructed modified direct evaporative cooling system. Table 1 shows the component parts of the system with their specifications.

The cooling pad

The cooling pad is a mixed media pad, made of luffa fiber lagged with charcoal. Luffa belongs to fruits of the species *luffa aegyptiaca and luffa acutangula*. The ripened

Fig. 3 Assembled system

Fig. 4 System mounted for test

Table 1 System component parts and specifications

S/No.	Part	Specification
1	Electric fan	Power consumption: 89 W, speed: 3.0 m/s
2	Wire mesh	Length: 0.36 m, width: 0.3 m
3	Dehumidifying pad	Length: 0.3 m, height: 0.36 m, thickness: 0.15 m
4	Rectangular channel	Face: (width: 0.3 m, height: 0.36 m), length: 0.4 m
5	Casing	Net dimensions: Length: 0.5 m, width: 0.4 m, height: 0.55 m
6	Water spray panel	Length: 0.32 m, width: 0.3 m, thickness: 0.003 m, Holes: 0.005 m
7	PVC pipe	Dia. 0.12 m
8	Cooling pad	Length: 0.3 m, height: 0.36 m, thickness: 0.32 m, face area: 0.108 m^2
9	Water pump	Power consumption: 0.2 hp, water flow rate: 0.07 L/s
10	Water refill pipe	Length: 0.05 m, dia. 0.25 m, thickness: 0.003 m
11	Water drain pipe	Length: 0.05 m, dia. 0.25 m, thickness: 0.003 m
12	Water tank	Length: 0.5 m, width: 0.35 m, height: 0.15 m, Volume: 0.02625 m^3, storage capacity 26.25 L

Table 2 Properties of the tamarind seed activated carbon granules

S/No.	Property	Value
1	Carbon yield (%)	47.8
2	Ash content (%)	13
3	Moisture content (%)	9.5
4	PH	6.5
5	Surface area (m^2/g)	952.77
6	Iodine no. (mg/g)	857

dry fibrous skeleton was used due to its porous nature and ability to retain water. Dry pieces of charcoal of equivalent diameter 0.03 m were embedded into the dry fibrous luffa skeleton. Charcoal was used because of its porous structure, which provides a very large adsorptive surface area. The luffa fiber lagged with charcoal were packed and held together by wire mesh according to the dimensions in Table 1.

The dehumidifying pad

The dehumidifying pad was made of tamarind seed activated carbon granules. The tamarind seed activated carbon granules was prepared by chemical activation, following the one step pyrolysis method. Crushed tamarind seed was impregnated with calcium carbonate ($CaCO_3$) in the ratio of 1:2. Carbonization was done at a furnace temperature of 600 °C, for thirty minutes. Properties of the tamarind seed activated carbon granules are given in Table 2. The granules were first wrapped loosely in plastic nets. The wrapped nets were then packed and held together using wire mesh according to the dimensions shown in Table 1. This made the pad very porous for free flow of air.

Experiment

In this section, the method employed in evaluating the space cooling energy demand and the experimental procedure are reported.

Space cooling energy demand calculation

The cooling space covers a total floor area of 12.95 m^2, with length, width and height of 3.7 × 3.5 × 3 m. The walls are made of bricks with plaster on both sides, while the roof is flat and made of concrete. The room has two double glazing windows of 3.24 m^2 area each. The room was modeled and simulated as a single zone using TRNSYS 16 software to determine the cooling energy demand. Weather data of Zaria, Nigeria, as contained in TRNSYS was used. Inputs which described the internal space, occupancy, equipment, and activity were specified in the model. The desired room temperature and relative humidity were set at 24 °C and 40% respectively. Simulation was done by computing the hourly cooling loads for each of the months, from which monthly peak cooling loads were obtained. The peak cooling load for the test room from TRNSYS simulation was 4.53 kW, this occurred in the month of April. Figure 5 shows the monthly peak cooling loads as well as the monthly average solar radiation.

Experimental procedure

Experimental performance evaluation of the modified direct evaporative cooling system was carried out. On the first experimental day, the dehumidifying pad was removed from the system; hence, the system operated with only the evaporative cooling section. On the second experimental day, the dehumidifying pad was fixed to the system, hence, the system operated by undergoing an evaporative cooling process and then the cooled moist air passed through the dehumidifying pad. Each of the experimental days lasted 9 h (from 8:30 am to 5:30 pm). The system was used to cool a room with a peak cooling load of 4.53 kW. At the start of each test day, the pump was put on to circulate water over the cooling pad for 10 min, without the fan operating. This was to ensure the cooling pad was properly wetted. After 10 min, the fan was then put on to suck in hot ambient air into the system. The resulting cooled air from the system cooled the test room. Temperature and humidity measurements at the ambient conditions and within the room were made. Room temperature and humidity measurements were made by

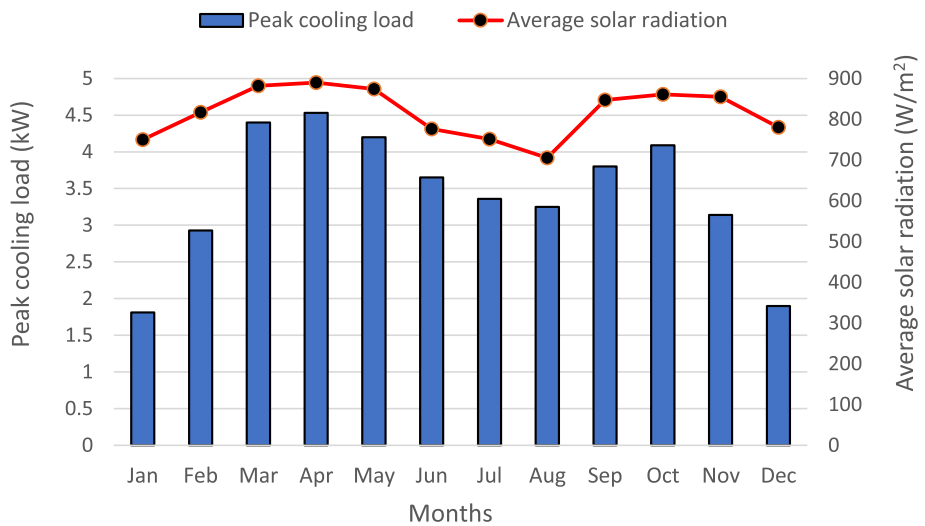

Fig. 5 Monthly peak cooling load and average solar radiation for the cooling space from TRNSYS simulation

taking readings at five different points within the room and then finding the average. The measurements made were those of ambient temperature, indoor dry bulb temperature, outdoor wet bulb temperature, outdoor relative humidity, indoor relative humidity, and water consumption. These measurements were made every 15 min. The water consumption was measured by reading off the height of the water level on the graduated water tank and then calculating the volume of the water consumed. The water in the tank was refilled with tap water once the water level dropped below half way. At the end of every experimental day, the entire tank water was drained and the tank filled with fresh water. While the dehumidifying pad was removed and dried in a solar dryer before being used in another experiment. An observation made on removing the dehumidifying pad for drying was that the luffa fiber became soaked and softened, an indication that material decay could result after prolonged use. The measuring instruments used for the temperature and humidity measurements with their specifications are as listed in Table 3.

Calculation of performance parameters

The following performance parameters as seen in equations 1, 2, 3 and 4 were calculated, using the relations according to Wang [31].

i. Cooling capacity: the cooling capacity was calculated using the following relation:

$$Q = \dot{m}_{air} C_p \left(T_{db,out} - T_{db,in}\right) \tag{1}$$

Where

$$\dot{m}_{air} = \rho v L H \tag{2}$$

ii. Cooling efficiency: the cooling efficiency was calculated using the following relation:

$$\eta = \frac{T_{db,out} - T_{db,in}}{T_{db,out} - T_{wb,out}} \tag{3}$$

iii. Coefficient of performance (COP): the COP was calculated using the following relation:

$$COP = \frac{Cooling\ capacity}{P_{fan} + P_{pump}} \tag{4}$$

iv. Water consumption: the water consumption was calculated as the difference in the volume of water in the tank between two successive measurement times as:

$$\text{Initial volume of water} - (h_w L_t W_t) \tag{5}$$

Table 3 Specification of measuring instruments

Parameter	Apparatus	Model. no.	Accuracy	Measuring range
Dry bulb temp.	Digital thermocouple thermometer	T407291	0.1 °C	− 50–1300 °C
Wet bulb temp.	Digital temperature humidity meter	Lunarlipes ST6817	0.1 °C	− 20–60 °C
Relative humidity	Digital humidity meter	1659454	3% RH	10% RH-99% RH

Uncertainty analysis

Uncertainty analysis for the experimental results presented in this study was carried out using the quadratic power method according to Kline [32], following the expressions in Eqs. 6 and 7:

$$\Delta F = \left[\left(\frac{\partial F}{\partial x_1} \right)^2 (\Delta x_1)^2 + \left(\frac{\partial F}{\partial x_2} \right)^2 (\Delta x_2)^2 \ldots .. + \left(\frac{\partial F}{\partial x_n} \right)^2 (\Delta x_n)^2 \right]^{\frac{1}{2}} \tag{6}$$

Where F is a function dependent on n variables, x represents the independent variable of the function, Δx is the uncertainty of the independent variable x, and ΔF is the uncertainty of the dependent variable F. The relative uncertainty of the dependent variable can be expressed as:

$$\frac{\Delta F}{F} = \left[\left(\frac{\partial F}{\partial x_1} \right)^2 \left(\frac{\Delta x_1}{F} \right)^2 + \left(\frac{\partial F}{\partial x_2} \right)^2 \left(\frac{\Delta x_2}{F} \right)^2 \ldots .. + \left(\frac{\partial F}{\partial x_n} \right)^2 \left(\frac{\Delta x_n}{F} \right)^2 \right]^{\frac{1}{2}} \tag{7}$$

For the present study, the relative uncertainty of the cooling efficiency and cooling capacity were respectively calculated in Eqs. (8) and (9) according to Kline [32], using Eq. (7) as

$$\frac{\Delta \eta}{\eta} = \left[\left(\frac{\partial \eta}{\partial T_{db,out}} \right)^2 \left(\frac{\Delta T_{db,out}}{\eta} \right)^2 + \left(\frac{\partial \eta}{\partial T_{db,in}} \right)^2 \left(\frac{\Delta T_{db,in}}{\eta} \right)^2 + \left(\frac{\partial \eta}{\partial T_{wb,out}} \right)^2 \left(\frac{\Delta T_{wb,out}}{\eta} \right)^2 \right]^{\frac{1}{2}} \tag{8}$$

$$\frac{\Delta Q}{Q} = \left[\left(\frac{\partial Q}{\partial T_{db,out}} \right)^2 \left(\frac{\Delta T_{db,out}}{Q} \right)^2 + \left(\frac{\partial Q}{\partial T_{db,in}} \right)^2 \left(\frac{\Delta T_{db,in}}{Q} \right)^2 \right]^{\frac{1}{2}} \tag{9}$$

Where the expressions for cooling efficiency and cooling capacity as given in Eqs. (3) and (1) respectively were used. The terms $\dot{m}_{air}$ (mass flow rate of air) and C_p(specific heat of air) in equation (1) are constant. The accuracy of measuring instrument as given in Table 3 was used. The results of the uncertainty analysis are shown in Table 4.

Results and discussion

Figure 6 shows the variation of ambient temperature, indoor dry bulb and outdoor wet bulb temperatures with time for experimental day 1. The ambient temperature is seen to increase from 26 °C at the start of the experiment to a maximum temperature of 36 °C between 13:00 and 14:00 h. It then decreases gradually to 28 °C at the end

Table 4 Results of uncertainty analysis

Performance parameter	Relative uncertainty (day 1)	Relative uncertainty (day 2)
Cooling efficiency	1.68%	1.69%
Cooling capacity	1.28%	1.41%

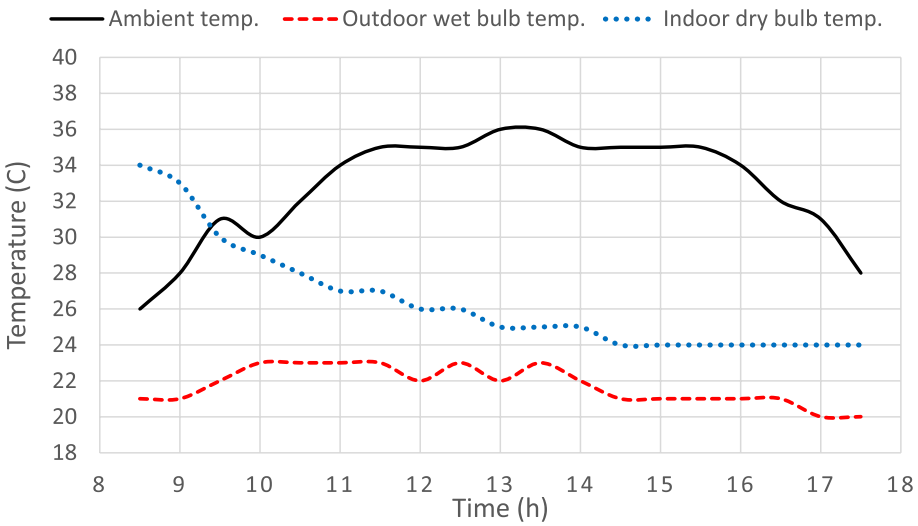

Fig. 6 Variation of temperatures with time for day 1

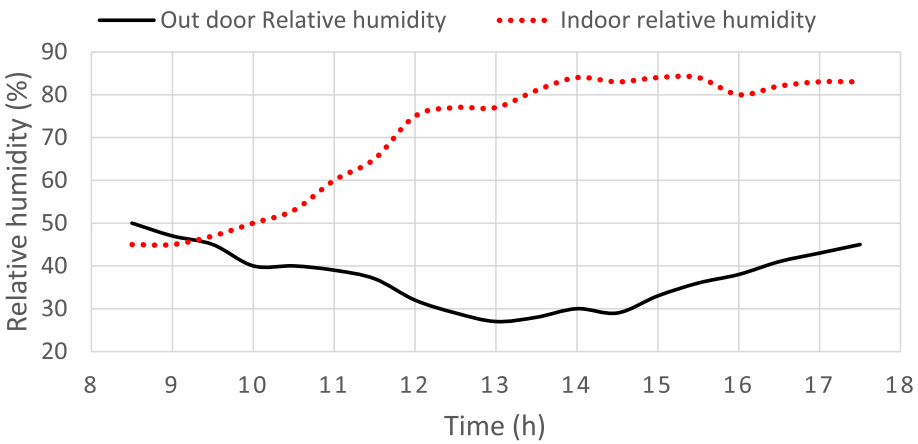

Fig. 7 Variation of outdoor and indoor relative humidity with time for day 1

of the experimental day. The indoor dry bulb temperature can be seen to decrease gradually from an initial temperature of 34 °C to 26 °C at noon. It decreases further to 24 °C at 14:30 h, then remains steady to the end of the experimental day. This indicates that space cooling was achieved, with a maximum temperature drop of 11 °C. Temperature drop of 10 °C was reported in the work of Awofa et al. [12]. The outdoor wet bulb temperature can be seen to fluctuate between 20 °C and 23 °C. The closest approach of the indoor dry bulb to outdoor wet bulb temperature is 2 °C.

Figure 7 shows the variation of outdoor and indoor relative humidity with time for experimental day 1. Note that the dehumidifying pad was not used on this day. It can be seen, that the outdoor relative humidity decreases from an initial value of 50% at the start of the experiment to a minimum of 27% at 13:00 h, from where it then rises to 45% at the end of the experiment. Comparing this with ambient temperature values in Fig. 6, an inverse relation is observed. Outdoor relative humidity is seen to decrease as ambient temperature increases and it increases as ambient temperature decreases. This is because increase in

ambient temperature causes much drier ambient air, thereby reducing the relative humidity. However, the indoor relative humidity is seen to increase from an initial value of 45% at the start of the experiment to 75% at noon. It further increases to 83% at the end of the experiment. This is due to the additional moisture introduced to the cooling space by the evaporative cooling process. Maximum recommended indoor relative humidity for human comfort in conditioned spaces is 65% [24]. Observing Fig. 7, it is seen that the indoor relative humidity exceeds 65% as from 11.5 h to the end of the experimental day, therefore making it unsuitable for human comfort. On observing Fig. 6, reduction in indoor temperature is seen, indicating sensible heat is being removed from the cooling space; however, latent heat is been introduced into the cooling space as indicated by rise in indoor relative humidity in Fig. 7. Increase in humidity of cooling space was reported in the work of Abaranji et al. [6], while Ibrahim et al. [11] reported increase in humidity of 30% in the cooling space.

Figure 8 shows the variation of cooling capacity and water consumption with time for experimental day 1. It can be observed that the cooling capacity increases gradually from the early hours (8.5 to 11.5 h), peaks at the mid-hours (12.5 to 15.5 h), then decreases towards the end hours (16.00 to 17.5 h). This is so because ambient temperatures are higher in the mid-day hours, as indicated in Fig. 6. This results in availability of high heat of vaporization which eventually causes evaporation and the air is cooled. A large temperature difference is created when cooling causes the indoor temperature to drop below the ambient temperature, leading to high cooling capacity. Maximum cooling capacity of 3.84 kW was achieved at 15.5 h. The water consumption can be seen to be lower in the early hours (8.5 to 11.5 h) and late hours (16.00 to 17.5 h), while it is seen to be higher in the mid-hours (12.00 to 15.5 h). This is because the outdoor relative humidity in the mid-hours is much lower than that of the early and late hours, as indicated in Fig. 7. The lower relative humidity allows for more evaporation of water into the ambient air, hence more water consumption. This also accounts for the higher cooling capacity recorded during this period, as heat is extracted from the air supplied to the evaporative cooling system to cause evaporation of water, which leads to cool air supply to the room, resulting to better performance. The total water consumed in the experimental day was 8.93 L, giving an average water consumption of 0.99 L/h for the day.

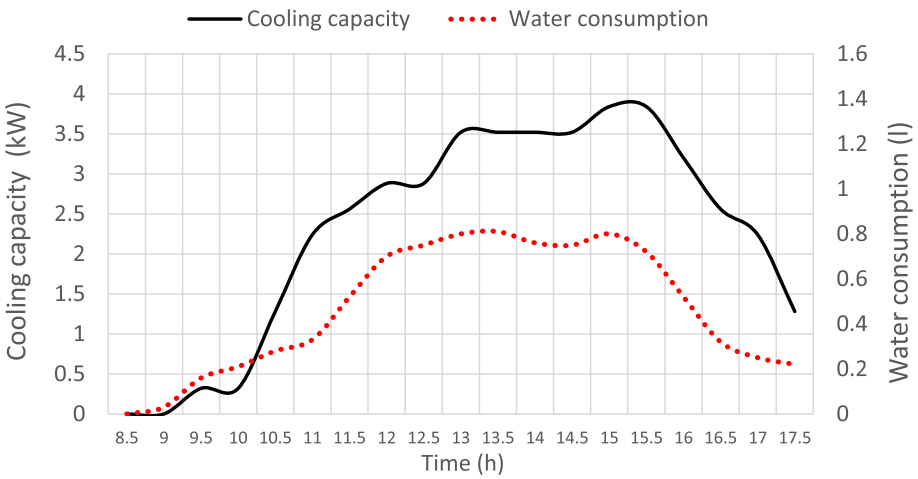

Fig. 8 Variation of cooling capacity and water consumption with time for day 1

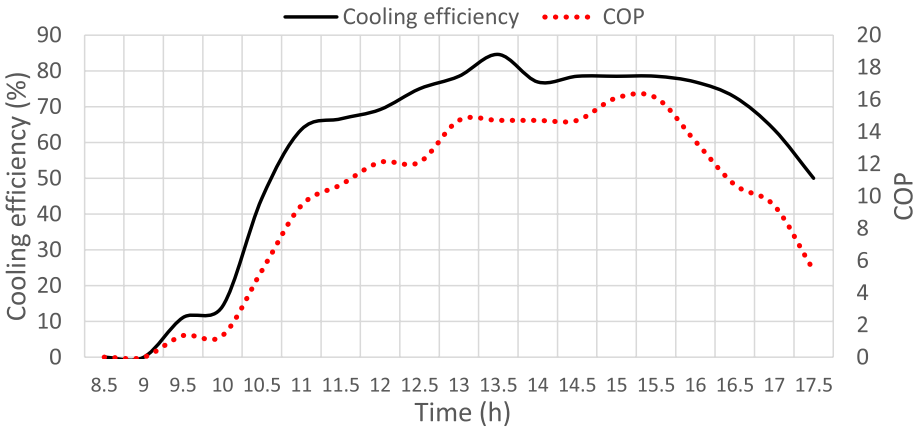

Fig. 9 Variation of cooling efficiency and COP with time for day 1

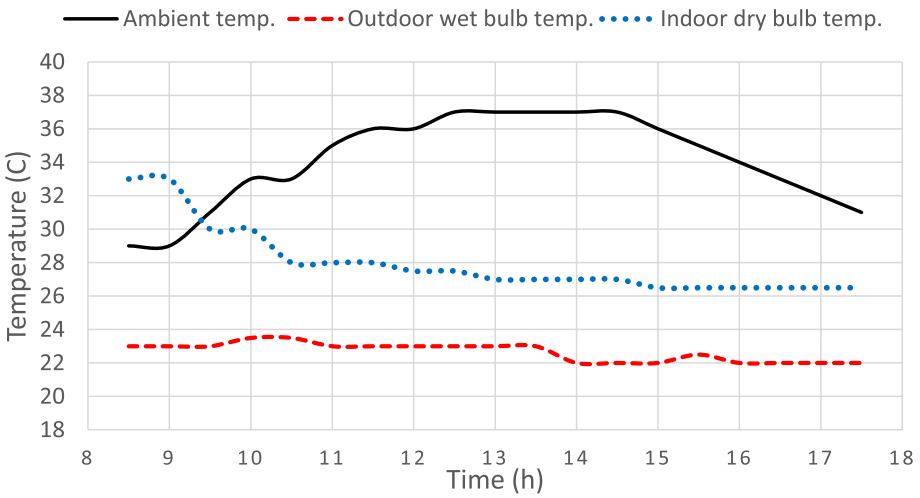

Fig. 10 Variation of temperatures with time for day 2

Figure 9 shows the variation of cooling efficiency and coefficient of performance with time for experimental day 1. The cooling efficiency and COP can be seen to increase from the start of the experiment to a peak between 12.00 h to 16.00 h, from where they begin to decrease till the end of the experimental day. The reason for the high efficiency within this period is because higher ambient temperatures are recorded within this period as indicated in Fig. 6. This causes large temperature difference between the ambient and indoor dry bulb temperatures when the space is cooled to lower temperatures, as well as closer approach to the outdoor wet bulb temperature, hence efficiency is higher. Also, because outdoor relative humidity is lower within this period, as indicated in Fig. 7, evaporation is enhanced, leading to higher cooling capacity and higher COP. Maximum efficiency of 84.6% was achieved at 13.5 h, while maximum COP of 16.1 was achieved at 15.5 h. COP of 4.05, 8.8 and 170 have been reported in the works of Dogramaci et al., Khosravi et al., and Nada et al. [15, 16, 19] respectively.

Results presented in Figs. 10, 11, 12, and 13 are those for the second experimental day, in which the dehumidifying pad was incorporated into the system. Figure 10 shows the

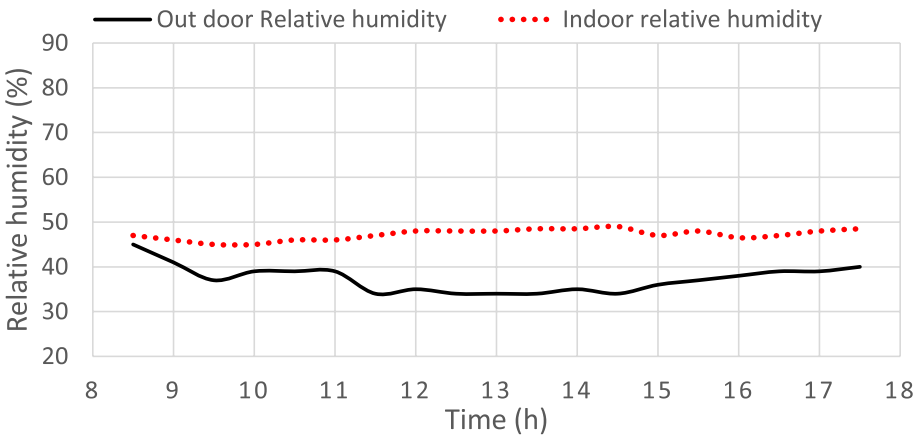

Fig. 11 Variation of outdoor and indoor relative humidity with time for day 2

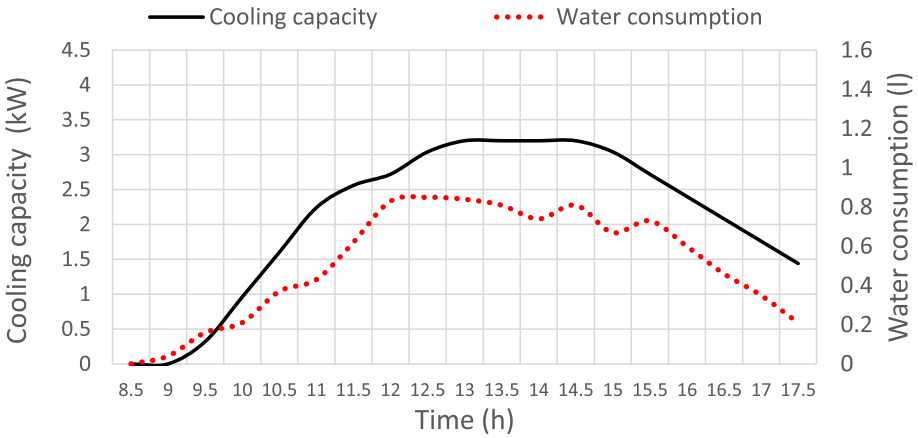

Fig. 12 Variation of cooling capacity and water consumption with time for day 2

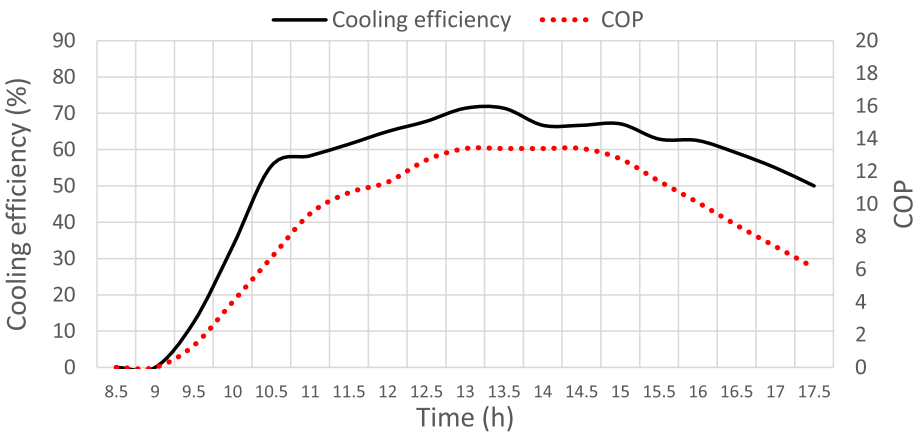

Fig. 13 Variation of cooling efficiency and COP with time for day 2

variation of ambient temperature, indoor dry bulb, and outdoor wet bulb temperatures with time for experimental day 2. The ambient temperature at the start of the experimental day is seen to be 27 °C. It increases gradually to a maximum temperature of 37

°C between 12.5 and 14.5 h, from where it then decreases to 31 °C at the close of the experimental day. The indoor dry bulb temperature is seen to decrease from an initial temperature of 33 °C at the start of the experiment to 27 °C at 13.00 h. It then decreases to 26.5 °C at 15.00 h, the room temperature is maintained at 26.5 °C to the end of the experimental day. This indicates that space cooling was achieved, with a maximum temperature difference of 10 °C between the ambient temperature and indoor dry bulb temperature. However, comparing the indoor dry bulb temperatures in Fig. 10 (with dehumidifying pad) to those in Fig. 6 (no dehumidifying pad), it is observed that the indoor dry bulb temperatures in Fig. 10 are a little higher. While the indoor dry bulb temperatures without the use of the dehumidifying pad eventually dropped to 24 °C, the indoor dry bulb temperatures when the dehumidifying pad was used were above 26 °C. This is due to the heat of adsorption introduced to the cooled air stream as it flows through the dehumidifying pad. Outdoor wet bulb temperatures were between 22 °C and 23.5 °C. Closest approach of oudoor dry bulb temperature to indoor wet bulb temperature was 4 °C.

Figure 11 shows the variation of outdoor and indoor relative humidity with time for experimental day 2. Note that the dehumidifying pad was used on the system for this day. From the figure, it can be seen that the outdoor relative humidity decreases from an initial 45% at the start of the experimental day to a minimum of 34% at 13.00 h. It then increases to 40% at the end of the experimental day. The indoor relative humidity at the start of the experiment can be seen to be 47%. A slight gradual increment in the indoor relative humidity can be observed until it attains 49% at 14.5 h. It then fluctuates from 46 to 49% till the end of the experimental day. This shows that minimal moisture was introduced to the room from the cooled air stream, an indication that the dehumidifying pad was able to absorb the moisture from the cooled moist air resulting from the evaporative cooling. Comparing the indoor relative humidity in Fig. 11 to that in Fig. 7, it would be observed that while the indoor relative humidity in Fig. 7 increased to above 80%, the indoor relative humidity in Fig. 11 remained below 50% throughout the experimental day. This is lower than the maximum indoor relative humidity of 65% recommended for human comfort in conditioned spaces [24]. This indicates that introduction of the dehumidifying pad was able to keep the indoor relative humidity within the range for human comfort.

Figure 12 shows the variation of cooling capacity and water consumption with time for experimental day 2. It can be observed that both cooling capacity and water consumption increase from the start of the day to attain the highest values between 12.00 and 15.5 h and then decrease till the end of the day. The relatively higher water consumption values between 12.00 and 15.5 h is due to the lower outdoor relative humidity recorded within this interval as seen from Fig. 11. This leads to better evaporation of water at the cooling pad, therefore performance of the system is enhanced. Peak cooling power of 3.2 kW was recorded between 13.00 and 14.5 h. This is lower than the peak cooling power of 3.84 kW recorded by the system without the dehumidifying pad as seen in Fig. 8. This is due to the rise in indoor dry bulb temperatures occasioned by the introduction of the dehumidifying pad. Total water consumption of 9.73 L was recorded for the experimental day, with an average water consumption of 1.08 L/h.

Figure 13 shows the variation of cooling efficiency and coefficient of performance with time for experimental day 2. The cooling efficiency is seen to increase from the start

of the experiment and attains higher values between 11.5 and 15.5 h. This is attributed to the high ambient temperatures recorded within this interval as seen from Fig. 10, which creates a wide temperature margin when the room temperature is cooled to lower values. Maximum cooling efficiency of 71.4% was attained between 13.00 and 13.5 h. Peak COP of 13.4 is seen to have been achieved between 13.00 and 14.5 h. These values are however lower than maximum values of 84.6% and 16.1 for the efficiency and COP respectively attained when the system operated without the dehumidifying pad. This is attributed to the higher indoor dry bulb temperatures recorded when the dehumidifying pad was used. Table 5 shows the comparison of cooling performance of the current study with those obtained from similar studies in literature. From the table, efficiency of 55.1% was achieved by Al–Suleiman et al. [13], while Laknizi et al. [17] achieved an efficiency of 56.9% using luffa fiber and pottery tubular rods respectively. Higher efficiencies were reported in the works of Korese and Hensel [20] (87.6%) and Velasco–Gomez et al. [18] (90%) using bulk charcoal and cotton fabric respectively. Efficiency from the current study which combined luffa fiber and charcoal can be seen to be 84.6% (without dehumidification) and 71.4% (with dehumidification). This is higher than that of Al–Suleiman [13] (55.1%) who used luffa fiber and compares favorably with that of Korese and Hensel [20], (87.6%) in which bulk charcoal was used. In general, it can be seen that the results from the current study fall favorably within the range of those from literature.

Conclusions

The performance of a modified evaporative cooling system which combines a cooling pad and a dehumidifying pad has been evaluated for space cooling. Results recorded for day 1, in which the dehumidifying pad was not used indicated a minimum space cooling temperature of 24 °C was achieved, giving a maximum temperature drop of 11 °C from ambient temperature. Indoor relative humidity however increased to 84%, which is above the range required for human comfort. Maximum cooling power and COP of 3.84 kW and 16.1 respectively were achieved, corresponding to ambient temperature of 36 °C, outdoor relative humidity of 33% and outdoor wet bulb temperature of 21 °C, while maximum cooling efficiency of 84.6% was achieved corresponding to ambient temperature of 36 °C, outdoor

Table 5 Comparison of cooling performance with different cooling pad materials

Pad material	Pad thickness (m)	Pad face area (m^2)	Air velocity (m/s)	Efficiency (%)	Reference
Luffa fiber	N/A	N/A	2.4	55.1	Al-Suleiman [13]
Jute	N/A	N/A	2.4	62.1	
Bulk charcoal	0.3	0.212	1.14	87.6	Korese and Hensel [20]
Vegetable loofah	0.125	0.931	0.773	57	De Melo et al. [21]
Cotton fabric	0.25	0.18	N/A	90	Velasco-Gomez et al. [18]
Corrugated cellulose paper	0.035	0.193	2.4	84	Nada et al. [19]
Pottery tubular rods	0.1	0.125	N/A	56.9	Laknizi et al. [17]
Luffa fiber + charcoal (no dehumidification)	0.32	0.108	3	84.6	Current study
Luffa fiber + charcoal (dehumidification)	0.32	0.108	3	71.4	

relative humidity of 28% and outdoor wet bulb temperature of 23 °C. Results for day 2 in which the dehumidifying pad was used showed a minimum room temperature of 26.5 °C was achieved, with a maximum temperature drop of 10 °C. Maximum indoor relative humidity of 49% was recorded, which falls within the range for human comfort. However, compared to system operation without the dehumidifying pad, lower values of maximum cooling power, COP and efficiency of 3.2 kW, 13.4 and 71.4% respectively were recorded, corresponding to ambient temperature of 37 °C, outdoor relative humidity of 34% and outdoor wet bulb temperature of 23 °C. These results show that the combination of the cooling pad and dehumidifying pad used in this work has been able to achieve sensible cooling as well as reduce the introduction of extra moisture to cooling space which is usually associated with direct evaporative cooling systems, thereby making it suitable for human comfort.

Abbreviations

COP	Coefficient of performance
PVC	Polyvinyl chloride
RH	Relative humidity
TRNSYS	Transient systems simulation program
C_p	Specific heat (J/kgK)
H	Height of pad (m)
h_w	Measured height of water in the tank (m)
L	Width of pad (m)
L_t:	Length of tank (m)
$\dot{m}_{air}$	Mass flow rate of air (kg/s)
P_{fan}	Power consumption of fan (kW)
P_{pump}	Power consumption of pump (kW)
Q	Cooling capacity (kW)
T	Temperature (K)
W_t	Width of tank (m)
db, in	Room dry bulb
db, out	Ambient dry bulb
wb, out	Ambient wet bulb
ρ	Density (kg/m^3)
v	Velocity of air (m/s)
η	Cooling efficiency

Acknowledgements
Not applicable

Authors' contributions
T. O. Ahmadu analyzed the readings and wrote the manuscript. Y. S. Sanusi conducted the experiment. F. Usman collected readings during the experiment. All authors read and approved the final manuscript.

Funding
This study had no funding from any source.

Availability of data and materials
The data used in the current study are available from the corresponding author on reasonable request.

Declarations

Competing interests
The authors declare that they have no competing interests.

Received: 18 March 2022 Accepted: 4 July 2022
Published online: 23 July 2022

References

1. Chan HY, Riffat SB, Zhu J (2010) Review of passive solar heating and cooling technologies. Renew Sust Energ Rev 14:781–789
2. Abas N, Kalair AR, Khan N, Haider A, Saleem Z, Saleem MS (2018) Natural and synthetic refrigerants, global warming: A review. Renew Sust Energ Rev 90:557–569

3. Chen X, Riffat S, Bai H, Zheng X, Reay D (2020) Recent progress in liquid desiccant dehumidification and air-conditioning: A review. Energy Built Environ 1:106–130
4. Sultan M, Miyazaki T, Koyama S (2018) Optimization of adsorption isotherm types for desiccant air-conditioning applications. Renew Energ 121:441–450
5. Glanville P, Kozlov A, Maisotsenko V (2011) Dew point evaporative cooling: Technology review and fundamentals. ASHRAE Transact 117:111–118
6. Abaranji S, Panchabikesan K, Ramalingam V (2020) Experimental investigation of a direct evaporative cooling system for year round thermal management with solar assisted dryer. Digital J. Int J Photoenergy 2020:6698904. https://doi.org/10.1155/2020/6698904
7. Lai L, Wang X, Kefayati G, Hu E (2021) Evaporative cooling integrated with solid desiccant systems: a review: Digital J. Energies 14:5982. https://doi.org/10.3390/en14185982
8. Rambhad K, Jondhale P, Kambale R, Jedhe V, Thakare K (2021) CFD analysis of solid desiccant dehumidifier wheel. International journal of analytical, experimental and finite element analysis. RAME Publishers 8(1):12–20
9. Frein A, Muscherà M, Scoccia R, Aprile M, Motta M (2018) Field testing of a novel hybrid solar assisted desiccant evaporative cooling system coupled with a vapour compression heat pump. Appl Therm Eng 130:830–846
10. Wang Y, Huang X, Li L (2018) Comparative study of the cross-flow heat and mass exchangers for indirect evaporative cooling using numerical methods. Digital J. Energies 11:3374. https://doi.org/10.3390/en11123374
11. Ibrahim E, Shao L, Riffat SB (2003) Performance of porous ceramic evaporators for building cooling application. Energ Build 35(9):941–949
12. Awofa EA, Nketsiah S, Alhassan M, Apiah-Kubi E (2020) Design, construction and performance evaluation of an evaporative cooling system for tomatoes storage. Sciendo Agric Eng 24(4):1–12
13. Al-Sulaiman F (2002) Evaluation of the performance of local fibres in evaporative cooling. Energ Conversion Manage 43(16):2267–2273
14. Jian JK, Hindoliya DA (2011) Experimental performance of new evaporative cooling pad materials. Sust Cities Soc 1(4):252–256
15. Dogramaci PA, Riffat S, Gan G, Aydin D (2019) Experimental study of the potential of eucalyptus fibres for evaporative cooling. Renew Energ 131:250–260
16. Khosravi N, Aydin D, Nejha MK, Dogramaci PA (2020) Comparative performance analysis of direct and desiccant assisted evaporative cooling systems using novel candidate materials. Digital J. Energ Conversion Manage 221:113167. https://doi.org/10.1016/j.enconman.2020.113167
17. Laknizi A, Abdellah AB, Faqir M, Essadiqi E, Dhimdi S (2021) Performance characterization of a direct evaporative cooling pad based on pottery material. Int J Sustain Energ 14(1):46–56
18. Velasco-Gómez E, Tejero-González A, Jorge-Rico J, Rey-Martínez FJ (2020) Experimental investigation of the potential of a new fabric-based evaporative cooling pad. Digital J. Sustainability 12:7070. https://doi.org/10.3390/su12177070
19. Nada SA, Elattar HF, Mahmoud MA, Fouda A (2020) Performance enhancement and heat and mass transfer characteristics of direct evaporative building free cooling using corrugated cellulose papers. Digital J. Energy 211(C). https://doi.org/10.1016/j.energy.2020.118678
20. Korese JK, Hensel O (2016) Experimental evaluation of bulk charcoal pad configuration on evaporative cooling effectiveness. Agric Eng Int CIGR J. 18(4):11–21
21. De Melo JFC, Bamberg JVM, Machado NS, Caldas ENG, Rodrigues MS (2019) Evaporative cooling efficiency of pads consisting of vegetable loofah. Comunicata Scientiae 10(1):38–44
22. Tejero-Gonzalez A, Franco-Salas A (2021) Optimal operation of evaporative cooling pads: A review. Digital J. Renew Sust Energ Rev 151:111632. https://doi.org/10.1016/j.rser.2021.111632
23. Singh RP, Mishra VK, Das RK (2018) Desiccant materials for air conditioning–a review. Digital J. IOP Conference Series 404:012005. https://doi.org/10.1088/1757-899X/404/1/012005
24. Zaher A, Elgendy E, Shabaan S (2020) An improved desiccant evaporative cooling system, parametric analysis and system comparison. Essam Elgendy/Engineering research journal 166:46–67
25. Narayanan R, Halawa E, Jain S (2018) Performance characteristics of solid desiccant evaporative cooling systems. Digital J. Energies 11:2574. https://doi.org/10.3390/en11102574
26. Dhamneya AK, Rajput SPS, Singh A (2018) Thermodynamic performance analysis of direct evaporative cooling system for increased heat and mass transfer area. Ain Shams Eng J 9:2951–2960
27. Sellami K, Feddaoui M, Labsi N, Najim M, Oubella M, Benkahla YK (2019) Direct evaporative cooling of ambient air using a ceramic wet porous layer. Chem Eng Res Design 142:225–236
28. Khater ESG (2014) Performance of direct evaporative cooling system under Egyptian conditions. J Climatol Weather Forecasting 2:119. https://doi.org/10.4172/2332-2594.1000119
29. He W, Xilian L, Yuhui S, Min Z, Zhaolin G (2018) Research of evaporative cooling experiment in summer of residential buildings in Xi'an. Energ Procedia 152:928–934
30. Hasani BH, Sohani A, Sayyaadi H, Karami R (2015) Acquiring the best cooling strategy based on thermal comfort and 3E analysis for small scale residential buildings at diverse climatic conditions. Int J Refrig 57:112–137
31. Wang SK (2001) Handbook of air conditioning and refrigeration, 2nd edn. McGraw – Hill companies Inc, U.S.A.
32. Kline SJ (1985) The purposes of uncertainty analysis. ASME J Fluids Eng 107(2):153–160

Publisher's Note